

# A new family of analytical anisotropic solutions by gravitational decoupling

Milko Estrada<sup>1,2,3,a</sup> and Francisco Tello-Ortiz<sup>1,b</sup>

<sup>1</sup> Departamento de Física, Facultad de ciencias básicas, Universidad de Antofagasta, Casilla 170, Antofagasta, Chile

<sup>2</sup> Instituto de Matemática, Física y Estadística, Universidad de las Américas, Manuel Montt 948, Providencia, Santiago, Chile

<sup>3</sup> Universidad Tecnológica de Chile, INACAP, Santiago, Chile

Received: 12 May 2018 / Revised: 26 August 2018

Published online: 6 November 2018

© Società Italiana di Fisica / Springer-Verlag GmbH Germany, part of Springer Nature, 2018

**Abstract.** This work is focused on the study of analytic anisotropic solutions to Einstein's field equations, describing spherically symmetric and static configurations by way of the gravitational decoupling through the method of minimal geometric deformation (MGD). For this we apply MGD to Heintzmann's solution obtaining two new analytic and well behaved anisotropic solutions, in which all their parameters such as the effective density, the effective radial and tangential pressure, as well as radial and tangential sound speed, fulfill each of the requirements for the physical acceptability available in the literature.

## 1 Introduction

In recent years great interest in the anisotropic solutions of Einstein's equations has emerged. This is so because the anisotropic scenarios describe some relevant astrophysical phenomena. Harko and Mak [1] showed some examples of this: nuclear matter may be anisotropic in certain high density ranges, or from the point of view of the Newtonian gravity, spherical galaxies can have anisotropic matter distribution. Harko and Mak in refs. [1, 2] argue that the interior of a star must fulfill the general physical conditions that describe a well behaved isotropic or anisotropic solution. Due to the later arguments, several models of anisotropic compact objects and its criteria have been studied in the literature [3–9].

According to the above-mentioned and other arguments, in recent years there has been a great interest in finding new anisotropic analytic solutions of Einstein equations, but this is not an easy task due the highly nonlinear behaviour of these equations (some examples of how to generate anisotropic solutions are exposed at refs. [10–12]). To address this problem, Ovalle [13], proposed a method called Minimal Geometric Deformation (MGD), which leads to finding new analytic anisotropic solutions of Einstein equations for spherically symmetric and static configurations. MGD was initially employed for the study of solutions at the braneworld scenarios [14, 15] and then this was spread to the study of black hole solutions [16, 17] (other applications can be seen in refs. [18–21]).

In this method the isotropic energy momentum tensor  $\bar{T}_{\mu\nu}$  is deformed by an additional source  $\Theta_{\mu\nu}$  whose coupling is proportional to the constant  $\alpha$ , and causes anisotropic effects on the self-gravitating system. This additional source can contain new fields, like scalar, vector and tensor fields [22]. However, in this work the source  $\Theta_{\mu\nu}$  will represent a generic gravitational source. Then the energy momentum tensor reads:

$$T_{\mu\nu} \mapsto \bar{T}_{\mu\nu} + \alpha\Theta_{\mu\nu}, \quad (1)$$

with the corresponding conservation equation

$$\nabla_{\nu}T^{\mu\nu} = 0. \quad (2)$$

Ovalle at ref. [22] argue “To summarise, the MGD-decoupling amounts to the following procedure: given two gravitational sources A and B, standard Einstein's equations are first solved for A, and then a simpler set of quasi-Einstein equations are solved for B. Finally, the two solutions can be combined in order to derive the complete solution for the

<sup>a</sup> e-mail: milko.estrada@ua.cl

<sup>b</sup> e-mail: francisco.tello@ua.cl

total system". The remarkable novelty of this method is that: one isotropic solution A is deformed and it produces a combined anisotropic solution  $A \cup B$  that preserves spherical symmetry. Due to the above explanation it is very interesting to apply MGD to an isotropic well behaved and spherically symmetric solution and then analyze the behavior of the new anisotropic solution (but now with an anisotropic criterion). Regarding this, in reference [23] one hundred twenty seven isotropic solutions were analyzed where only 9 of them were well behaved from the physical point of view.

One interesting isotropic spherically symmetric solution is the Heintzmann's space-time [24]. In ref. [23] it was shown that this solution is well behaved for an arbitrary election of the constants (specifically the special case in which the constants  $a$ ,  $c$  and  $A$  have magnitude equal to 1 in eq. (25)). In this work we will show that this solution is still well behaved for the values of mass and radii of physical interest described below. These values yield to values of constants  $a$  and  $c$  that are no longer restricted to be equal to one. Heintzmann's solution has been extended to an anisotropic charged case in refs. [25,26] also showing that it is a well behaved solution.

Furthermore, in this work we will analyze the minimal geometric deformation of the isotropic Heintzmann's solution and we will get two new anisotropic solutions. The matching conditions are obtained with the Schwarzschild exterior solution and then we will study the physical admissibility of these new solutions. For this, we will use realistic values of radii and mass that correspond to the stars 4U 1538-52, RXJ 1856-37 and Vela X-1 [8,9], again these values of mass and radii will lead to values of the constants  $a$  and  $c$  that are no longer restricted to be equal to one.

This work is organized as follows: Section 2 presents the Einstein equations for the energy momentum tensor (1); in sect. 3 we explain the MGD method in more detail; in sect. 4 we study the physical acceptability of the isotropic Heintzmann's solution for typical values of radius and mass of some compact objects. Section 5 is devoted to the application of the MGD method to the Heintzmann's solution, showing two new anisotropic physically acceptable solutions; finally, sect. 6 summarizes the essentials of this work and exposes some conclusions.

## 2 Einstein's field equations for multiple sources

Starting with the standard Einstein's equations:

$$G_{\mu\nu} \equiv R_{\mu\nu} - \frac{1}{2}Rg_{\mu\nu} = -\kappa^2 T_{\mu\nu}, \tag{3}$$

where  $T_{\mu\nu}$  is given by (1) and  $\bar{T}_{\mu\nu}$  corresponds to a perfect fluid,

$$\bar{T}_{\mu\nu} = (\bar{\rho} + \bar{p}) u_\mu u_\nu - \bar{p} g_{\mu\nu}, \tag{4}$$

being  $u^\mu$  the four-velocity,  $\bar{\rho}$  and  $\bar{p}$  the density and the isotropic pressure, respectively.

In Schwarzschild coordinates the spherically symmetric line element reads:

$$ds^2 = e^{\nu(r)} dt^2 - e^{\lambda(r)} dr^2 - r^2 (d\theta^2 + \sin^2 \theta d\phi^2), \tag{5}$$

where  $\nu = \nu(r)$  and  $\lambda = \lambda(r)$  are purely radial functions and  $r$  ranging from  $r = 0$  (the object center) to  $r = R$  (the object surface). The line element (5) satisfy the Einstein's equation (3), which leads to:

$$\kappa^2 (\bar{\rho} + \alpha \Theta_0^0) = \frac{1}{r^2} - e^{-\lambda} \left( \frac{1}{r^2} - \frac{\lambda'}{r} \right), \tag{6}$$

$$\kappa^2 (\bar{p} - \alpha \Theta_1^1) = -\frac{1}{r^2} + e^{-\lambda} \left( \frac{1}{r^2} + \frac{\nu'}{r} \right), \tag{7}$$

$$\kappa^2 (\bar{p} - \alpha \Theta_2^2) = \frac{e^{-\lambda}}{4} \left( 2\nu'' + \nu'^2 - \lambda'\nu' + 2\frac{\nu' - \lambda'}{r} \right). \tag{8}$$

The conservation equation (2), which is a linear combination of eqs. (6)–(8), yields:

$$\bar{p}' + \frac{\nu'}{2}(\bar{\rho} + \bar{p}) - \alpha(\Theta_1^1)' + \frac{\nu'}{2}\alpha(\Theta_0^0 - \Theta_1^1) + \frac{2\alpha}{r}(\Theta_2^2 - \Theta_1^1) = 0. \tag{9}$$

Here the prime means differentiation respect to  $r$ . So, the perfect fluid is recovered in the limit  $\alpha \rightarrow 0$ .

In order to simplify the above system, we identify the effective density, the effective radial and tangential pressures as

$$\rho = \bar{\rho} + \alpha \Theta_0^0, \tag{10}$$

$$p_r = \bar{p} - \alpha \Theta_1^1, \tag{11}$$

$$p_t = \bar{p} - \alpha \Theta_2^2, \tag{12}$$

where in the extra fluid  $\Theta_1^1 \neq \Theta_2^2 = \Theta_3^3$ . So the total anisotropy introduced by the generic source  $\Theta_{\mu\nu}$  is given by

$$\Pi \equiv p_t - p_r = \alpha (\Theta_1^1 - \Theta_2^2). \tag{13}$$

### 3 Minimal geometric deformation method

This method for spherically symmetric distributions was proposed in refs. [13, 22]. We will begin by considering a solution to eqs. (6)–(8) with  $\alpha = 0$ , namely, a GR perfect fluid solution  $\{\eta, \mu, \bar{\rho}, \bar{p}\}$ , where  $\eta$  and  $\mu$  are the corresponding metric functions:

$$ds^2 = e^{\eta(r)} dt^2 - \mu(r)^{-1} dr^2 - r^2 d\Omega^2. \tag{14}$$

Turning on the parameter  $\alpha$  we can see the effects of the source  $\Theta_{\mu\nu}$  on the perfect fluid solution  $\{\eta, \mu, \bar{\rho}, \bar{p}\}$ . These effects can be encoded in the geometric deformation undergone by the perfect fluid geometry  $\{\eta, \mu\}$  in eq. (14) as follows:

$$\mu(r) \mapsto e^{-\lambda(r)} = \mu(r) + \alpha f^*(r), \tag{15}$$

$$\eta(r) \mapsto \nu(r) = \eta(r); \tag{16}$$

it means that only the radial component of the line element (14) is deformed, where  $f^*(r)$  is the corresponding deformation to the radial part. Upon replacing eqs. (15) and (16) in the Einstein equations (6)–(8), the system splits into two sets of equations:

- 1) The standard Einstein equations for a perfect fluid (with  $\alpha = 0$ ), where  $\eta(r) = \nu(r)$ ,

$$\kappa^2 \bar{\rho} = \frac{1}{r^2} - \frac{\mu}{r^2} - \frac{\mu'}{r}, \tag{17}$$

$$\kappa^2 \bar{p} = -\frac{1}{r^2} + \mu \left( \frac{1}{r^2} + \frac{\nu'}{r} \right), \tag{18}$$

$$\kappa^2 \bar{p} = \frac{\mu}{4} \left( 2\nu'' + \nu'^2 + 2\frac{\nu'}{r} \right) + \frac{\mu'}{4} \left( \nu' + \frac{2}{r} \right), \tag{19}$$

along with the conservation equation (2) with  $\alpha = 0$ , namely,  $\nabla_\nu \bar{T}^{\mu\nu}$ , yielding

$$\bar{p}' + \frac{\nu'}{2} (\bar{\rho} + \bar{p}) = 0, \tag{20}$$

which is a linear combination of eqs. (17)–(19).

- 2) The terms of order  $\alpha$  give rise to the following *quasi-Einstein equations* [13, 22], which include the source  $\Theta_{\mu\nu}$ :

$$\kappa^2 \Theta_0^0 = -\frac{f^*}{r^2} - \frac{f^{*'}}{r}, \tag{21}$$

$$\kappa^2 \Theta_1^1 = -f^* \left( \frac{1}{r^2} + \frac{\nu'}{r} \right), \tag{22}$$

$$\kappa^2 \Theta_2^2 = -\frac{f^*}{4} \left( 2\nu'' + \nu'^2 + 2\frac{\nu'}{r} \right) - \frac{f^{*'}}{4} \left( \nu' + \frac{2}{r} \right). \tag{23}$$

The conservation equation (2) then yields to  $\nabla_\nu \Theta^{\mu\nu} = 0$ , which explicitly reads:

$$(\Theta_1^1)' - \frac{\nu'}{2} (\Theta_0^0 - \Theta_1^1) - \frac{2}{r} (\Theta_2^2 - \Theta_1^1) = 0. \tag{24}$$

It is worth stressing that eqs. (20) and (24) imply that there is no exchange of energy momentum between the perfect fluid and the extra source  $\Theta_\nu^\mu$ . So there is only purely gravitational interaction.

### 4 Heintzmann’s solution

In this section we will analyze if the isotropic Heintzmann’s solution [24] is still well behaved for our physical interest parameters of mass and radii, these correspond to the stars 4U 1538-52, RXJ 1856-37 and Vela X-1 [8, 9]. In ref. [23] this solution is called as Heint IIa. The line element is

$$ds^2 = A^2 (1 + ar^2)^3 dt^2 - \left( 1 - \frac{3ar^2}{2} \frac{1 + c(1 + 4ar^2)^{-1/2}}{1 + ar^2} \right)^{-1} dr^2 - r^2 d\Omega^2, \tag{25}$$

where  $a$ ,  $c$  and  $A$  are constant parameters. The pressure  $\bar{p}$  and the energy density  $\bar{\rho}$  are

$$\bar{p}(r) = -\frac{3a[(3ar^2 - 3)(1 + 4ar^2)^{1/2} + c(1 + 7ar^2)]}{2\kappa^2(4ar^2 + 1)^{1/2}(1 + ar^2)^2}, \quad (26)$$

$$\bar{\rho}(r) = \frac{3a[(4a^2r^4 + 13ar^2 + 3)(1 + 4ar^2)^{1/2} + 3c + 9acr^2]}{2\kappa^2(4ar^2 + 1)^{1/2}(1 + ar^2)^2}. \quad (27)$$

#### 4.1 Coupling with Schwarzschild exterior solution

We will present the conditions for the coupling of isotropic solution (25) with the Schwarzschild vacuum exterior solution:

$$ds^2 = \left(1 - \frac{2\bar{M}}{r}\right) dt^2 - \left(1 - \frac{2\bar{M}}{r}\right)^{-1} dr^2 - r^2 d\Omega^2. \quad (28)$$

For this, we will take into account the Israel-Darmois matching conditions. At the stellar surface  $\Sigma$  defined by  $r = R$  these conditions give [27]

$$[G_{\mu\nu}r^\nu]_\Sigma = 0, \quad (29)$$

where  $r_\nu$  is a unit radial vector and  $[F]_\Sigma \equiv F(r \rightarrow R^+) - F(r \rightarrow R^-)$ , for any function  $F = F(r)$ . Using eq. (29) and the general Einstein equations, we find that

$$[\bar{T}_{\mu\nu}r^\nu]_\Sigma = 0, \quad (30)$$

which leads to

$$[\bar{p}]_\Sigma = 0, \quad (31)$$

because in the external vacuum Schwarzschild solution the pressure is zero, then the last equation yields

$$\bar{p}(R) = 0. \quad (32)$$

Using eq. (26), we find the value of the constant  $c$  from eq. (32)

$$c = \frac{3(1 + 4aR^2)^{1/2}(1 - aR^2)}{1 + 7aR^2}. \quad (33)$$

The second condition, also given by the Israel-Darmois conditions, says that the line element must be continuous, *i.e.* there must be no jumps in the metric,

$$[ds^2]_\Sigma = 0, \quad (34)$$

so,

$$g_{tt}^-(R) = g_{tt}^+(R) \quad (35)$$

and

$$g_{rr}^-(R) = g_{rr}^+(R), \quad (36)$$

where  $g_{tt}$  and  $g_{rr}$  are the temporal and radial components of the metric. Then equating (25) with (28) and using the conditions (35) and (36) we get:

$$A^2 (1 + aR^2)^3 = 1 - \frac{2\bar{M}}{R}, \quad (37)$$

$$1 - \frac{3aR^2}{2} \frac{1 + c(1 + 4aR^2)^{-1/2}}{1 + aR^2} = 1 - \frac{2\bar{M}}{R}. \quad (38)$$

We will take  $\bar{M}$  and  $R$  as free parameters. Inserting the parameter  $c$  from eq. (33) into eq. (38), we find:

$$a = \frac{\bar{M}}{R^2(3R - 7\bar{M})}, \quad (39)$$

then with this value for  $a$  we obtain the value for  $c$  from eq. (33) and for  $A$  from eq. (37).

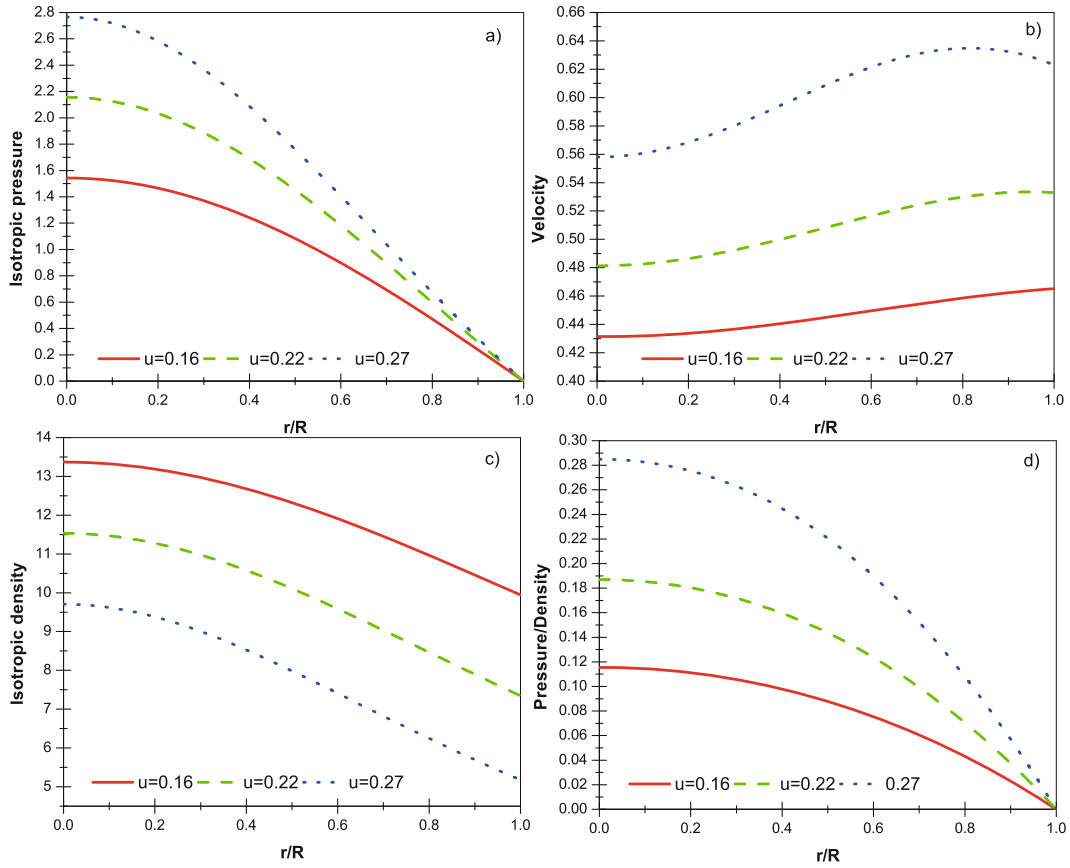


**Fig. 1.** Panel (a) shows the isotropic pressure which vanishes at the boundary  $r = R$ . Panel (b) shows that the sound speed velocity obeys causality condition  $v_s \leq 1$ . Panel (c) exhibits the monotonically decreasing behaviour of the density with increasing  $r$ . Finally panel (d) shows the decreasing pressure-density ratio  $\bar{p}/\bar{\rho}$ . In the graphics the pressure and density are divided by the value of  $a$ . These plots correspond to the solution of sect. 4.

The criteria for the physical admissibility are well known (as an example see ref. [23]), and could represent a particular case of the conditions of subsect. 5.1 when  $p_r = p_t$  (excluding the energy momentum tensor conditions). In this work we will choose the following values of mass and radius:  $\bar{M} = 0.87$  solar mass and  $R = 7.866$  km with a compactness factor  $u = \bar{M}/R = 0.16$ ;  $\bar{M} = 0.9041$  solar mass and  $R = 6$  km with a compactness factor  $u = \bar{M}/R = 0.22$  and  $\bar{M} = 1.77$  solar mass and  $R = 9.56$  km with a compactness factor  $u = \bar{M}/R = 0.27$  (these values are typical of compact objects. Indeed these correspond to the stars 4U 1538-52, RXJ 1856-37 and Vela X-1, respectively [8, 9]). With these values we obtain the constants  $a$ ,  $c$  and  $A$  from eqs. (39), (33) and (37). In fig. 1 we observe that in the three cases the density and pressure are positive and decreasing, the pressure vanishes at the boundary and the square of light velocity is less than 1 (for simplicity in the graphic analysis we take  $\kappa = 1$ ). Therefore Heintzmann’s solution is well behaved under our physical assumptions. Throughout the text  $u$  represents in all figures the mass-radius ratio.

### 5 Applying MGD to Heintzmann’s solution

In this section we will apply the MGD method to Heintzmann’s solution and we will obtain two new analytic solutions. Furthermore, we will test if these new solutions are well behaved from the physical point of view; to do this we will use realistic values of mass and radii that correspond to the stars 4U 1538-52, RXJ 1856-37 and Vela X-1 [8, 9].

From eq. (25) we have:

$$e^{\nu(r)} = A^2 (1 + ar^2)^3, \tag{40}$$

$$\mu(r) = 1 - \frac{3ar^2}{2} \frac{1 + c(1 + 4ar^2)^{-1/2}}{1 + ar^2}. \tag{41}$$

Now we apply the MGD method to Heintzmann's solution (25). Following eqs. (15) and (16) we get:

$$e^{\nu(r)} = A^2 (1 + ar^2)^3, \quad (42)$$

$$e^{-\lambda(r)} = 1 - \frac{3ar^2}{2} \frac{1 + c(1 + ar^2)^{-1/2}}{1 + ar^2} + \alpha f^*(r), \quad (43)$$

where  $f^*(r)$  is determined by imposing a mimic constraint on the density or pressure. With respect to this, two choices leading to physically acceptable solutions are following mimic constraints [21, 22]:

$$\Theta_0^0(r) = \bar{\rho}(r), \quad (44)$$

or

$$\Theta_1^1(r) = \bar{p}(r). \quad (45)$$

As soon as any mimic constraint (44) or (45) is imposed,  $f^*(r)$  can be determined. With respect to the constant parameters  $a$ ,  $c$  and  $A$ , they are determined matching the expressions (42) and (43) with the corresponding Schwarzschild's exterior solution:

$$ds^2 = - \left(1 - \frac{2M}{r}\right) dt^2 + \left(1 - \frac{2M}{r}\right)^{-1} dr^2 + r^2 d\Omega^2. \quad (46)$$

The first matching condition is given by eqs. (29) and (11), obtaining:

$$p_r(R) = 0, \quad (47)$$

so,

$$\bar{p}(R) - \alpha \Theta_1^1(R) = 0. \quad (48)$$

The second matching condition is given by eq. (34), yielding to

$$A^2 (1 + aR^2)^3 = 1 - \frac{2M}{R} \quad (49)$$

and

$$\left(1 - \frac{3aR^2}{2} \frac{1 + c(1 + 4aR^2)^{-1/2}}{1 + aR^2}\right) + \alpha f^* = 1 - \frac{2M}{R}. \quad (50)$$

Equating eqs. (49) and (50) we obtain

$$A^2 (1 + aR^2)^3 = \left(1 - \frac{3aR^2}{2} \frac{1 + c(1 + 4aR^2)^{-1/2}}{1 + aR^2}\right) + \alpha f^*. \quad (51)$$

## 5.1 Admissibility of the solution

On the other hand, when one considers an anisotropic matter distribution the basic requirements change slightly; these are given by refs. [1, 2, 28]:

- 1) The density and pressure  $p_r$  should be positive inside the star.
- 2) The gradients  $d\rho/dr$ ,  $dp_r/dr$  and  $dp_t/dr$  should be negative.
- 3) Inside the static configuration the speed of sound should be less than the speed of light, *i.e.*,  $0 \leq dp_r/d\rho \leq 1$  and  $0 \leq dp_t/d\rho \leq 1$ .
- 4) A physically reasonable energy-momentum tensor has to obey the conditions  $\rho - p_r - 2p_t \geq 0$  and  $\rho + p_r + 2p_t \geq 0$ .
- 5) The radial pressure must vanish but the tangential pressure may not vanish at the boundary  $r = R$  of the sphere. However, the radial pressure is equal to the tangential pressure at the center of the fluid sphere.

In this article we will analyze the above criteria. However, some of these requirements are still in discussion, for example in [29] it has been claimed that a solution which disrupts the condition 3) could still be allowed.

Other authors argued that the speed of sound must decrease with increasing  $r$ . But the latest assumption could not be valid for an anisotropic fluid, since the speed of sound at the isotropic case could be directly related to the material rigidity. In fact, it is expected that stable configurations have a greater rigidity inside and that it decrease with increasing  $r$ , *i.e.* the sound speed should be decreasing as increasing  $r$ . But the latest assumption is not mandatory for anisotropic fluids [30].

With respect to item 1), some authors have argued that if ordinary matter is present, described by a high density state equation, in which anisotropies naturally appear, one should impose the condition of the positivity of all pressures. However, for more exotic types of matter (dark energy, or as in our case: scalar or vectorial fields, or generic gravitational sources, etc.) the tangential pressure may be negative inside the star, and it may not vanish on the surface. Exotic objects like compact gravastars or compact boson stars could have negative pressures [31].

### 5.2 Solution I: Mimic constraint for pressure

We will use the constraint (45), so from eq. (11) we get the following value for the effective radial pressure:

$$p_r = (1 - \alpha)\bar{p}(r), \tag{52}$$

where  $\bar{p}(r)$  is given by eq. (26).

Equating eqs. (18) and (22) we obtain the following expression for  $f^*(r)$ :

$$f^*(r) = \frac{3ar^2}{2} \frac{1 + c(1 + 4ar^2)^{-1/2}}{1 + ar^2} + \frac{ar^2 + 1}{7ar^2 + 1} - 1. \tag{53}$$

Hence from eq. (43) the deformed radial metric component reads:

$$e^{-\lambda(r)} = (1 - \alpha)\mu(r) + \alpha \left( \frac{ar^2 + 1}{7ar^2 + 1} \right), \tag{54}$$

where  $\mu(r)$  corresponds to eq. (41). The interior metric functions given by eqs. (42) and (54) represent the Heintzmann’s solution minimally deformed by the generic anisotropic source  $\Theta_{\mu\nu}$ . We can see that the limit  $\alpha \rightarrow 0$  in eq. (54) leads to the standard Heintzmann’s solution for a perfect fluid.

At this point, we will match the deformed interior metric given by (42) and (54), with the exterior vacuum Schwarzschild solution (46). Using (47), and since  $\alpha \neq 0$  in eq. (52) we arrive at

$$\bar{p}(R) = 0, \tag{55}$$

which, according to eq. (26) leads to

$$c = \frac{3(1 + 4aR^2)^{1/2}(1 - aR^2)}{1 + 7aR^2}. \tag{56}$$

The continuity of the metric is given by eqs. (49) and (50):

$$A^2 (1 + aR^2)^3 = 1 - \frac{2M}{R} \tag{57}$$

and

$$(1 - \alpha)\mu(r) + \alpha \left( \frac{ar^2 + 1}{7ar^2 + 1} \right) = 1 - \frac{2M}{R}. \tag{58}$$

Equations (56), (57) and (58) are the necessary and sufficient conditions to match the interior solution with the exterior Schwarzschild space-time.

We will evaluate  $c$  from eq. (56) at eq. (58) and we get the following expression for  $a$ :

$$a = \frac{M}{R^2(3R - 7M)}. \tag{59}$$

Then with the above expression (59), we will obtain the value for  $c$  from eq. (56) and for  $A$  from eq. (57).

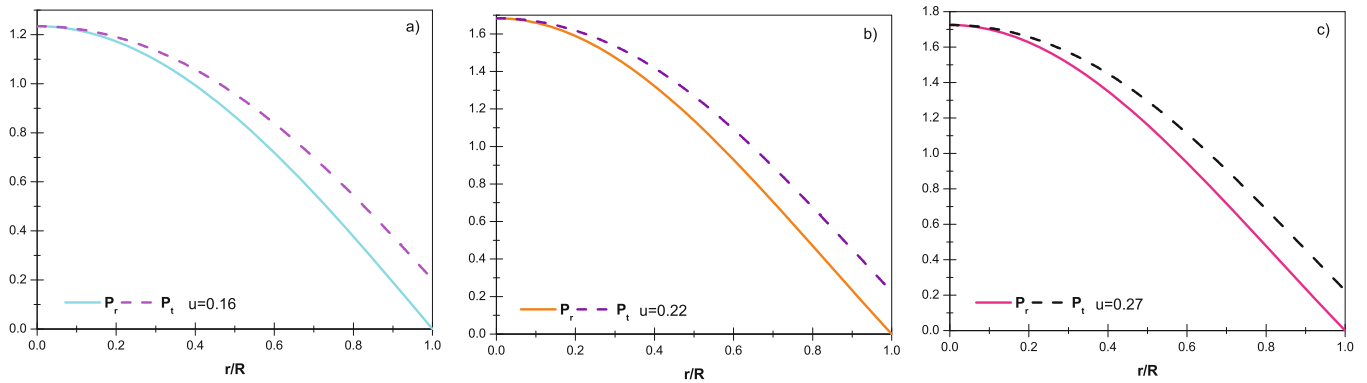


**Fig. 2.** The three panels display the radial (lower curve) and the tangential (upper curve) pressures, exhibiting a monotonically decreasing behaviour with the increasing  $r$ . All the above quantities are divided by  $a$ , i.e.  $P_r = p_r/a$  and  $P_t = p_t/a$ . These plots correspond to the solution of subject. 5.2 with  $\alpha = 0.2$ .

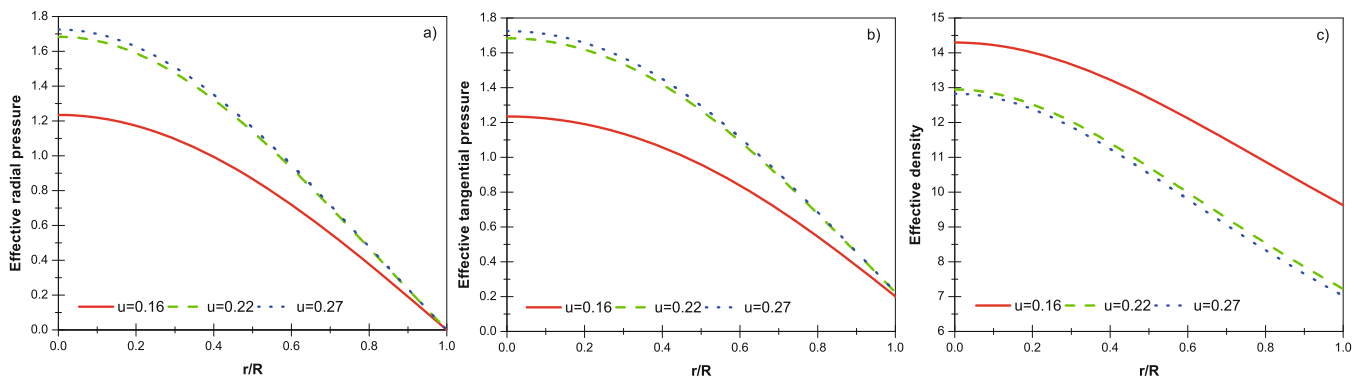


**Fig. 3.** Panel (a) shows the effective radial pressure. Panel (b) shows the effective tangential pressure and panel (c) shows the decreasing effective energy density. All these quantities are normalized by  $a$ . These plots correspond to the solution of subject. 5.2 with  $\alpha = 0.2$ .

On the other hand, by replacing  $f^*(r)$  given by (53) in eqs. (21) and (23), we obtain  $\Theta_0^0(r)$  and  $\Theta_2^2(r)$ :

$$\Theta_0^0(r) = -\frac{9a}{2\kappa^2} \frac{\zeta(r)}{(ar^2 + 1)^2(7ar^2 + 1)^2(4ar^2 + 1)^{3/2}}, \tag{60}$$

$$\Theta_2^2(r) = -\frac{3a}{2\kappa^2} \frac{\xi(r)}{(ar^2 + 1)^2(7ar^2 + 1)^2(4ar^2 + 1)^{1/2}}, \tag{61}$$

where the functions  $\zeta(r)$  and  $\xi(r)$  are

$$\zeta(r) = \sqrt{1 + 4ar^2} (-3 - 15ar^2 + 19a^2r^4 + 131a^3r^6 + 28a^4r^8) + 17car^2 + 91a^2r^4c + 147a^3r^6c + c, \tag{62}$$

$$\xi(r) = \sqrt{1 + 4ar^2} (189a^3r^6 - 45a^2r^4 - 21ar^2 - 3) + 343a^3r^6c + 147a^2r^4c + 21car^2 + c. \tag{63}$$

The above expressions allow us to find the effective density and the effective tangential pressure from eqs. (10) and (12):

$$\rho(r) = \bar{\rho}(r) - \frac{\alpha}{2\kappa^2} \frac{9a\zeta(r)}{(ar^2 + 1)^2(7ar^2 + 1)^2(4ar^2 + 1)^{3/2}} \tag{64}$$

$$p_t(r) = \bar{p}(r) + \frac{\alpha}{2\kappa^2} \frac{3a\xi(r)}{(ar^2 + 1)^2(7ar^2 + 1)^2(4ar^2 + 1)^{1/2}}. \tag{65}$$

From the physical admissibility analysis we will fix as free parameters the constants  $M$  and  $R$  corresponding again to the same values of mass and radius above declared in sect. 4. We evaluate at eq. (59) and obtain the value of  $a$  and, from eq. (56), we obtain the value of  $c$ . In figs. 2, 3, 4 and 5 we see that all conditions from physical admissibility of subject. 5.1 are satisfied.



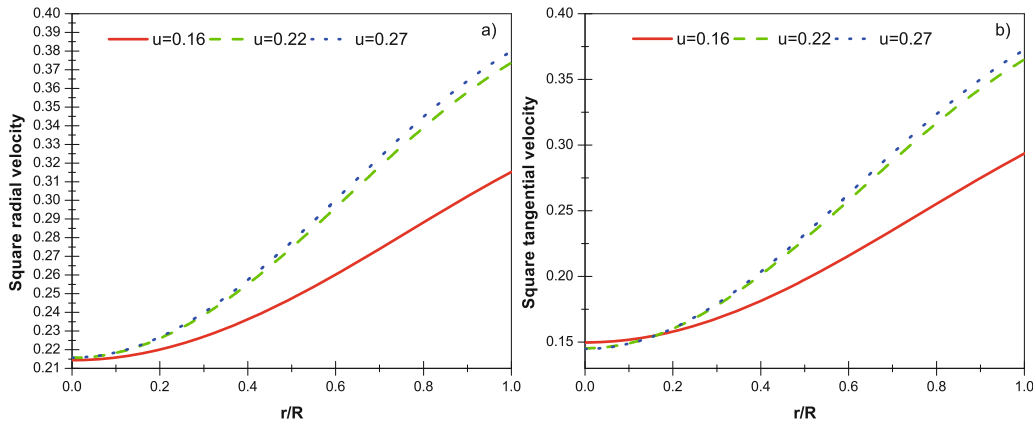


**Fig. 4.** Panels (a) and (b) show the squares of radial and tangential velocities, respectively. These plots correspond to the solution of subject. 5.2 with  $\alpha = 0.2$ .

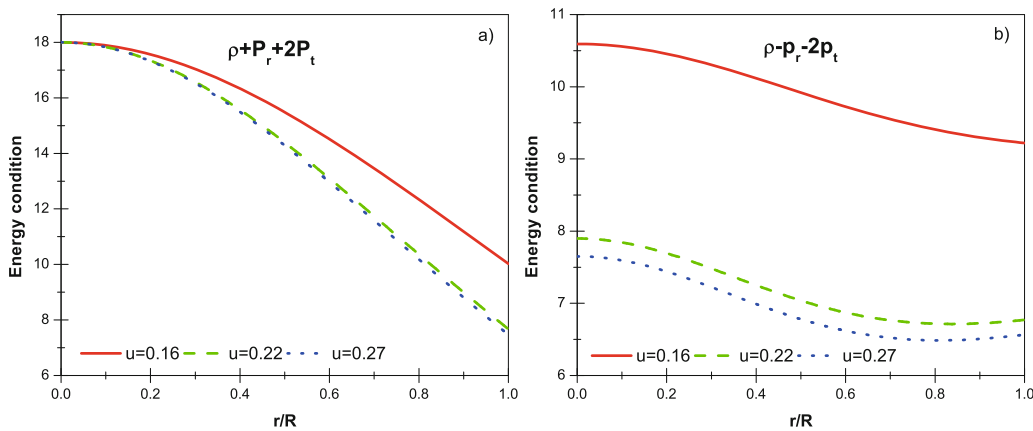


**Fig. 5.** Panels (a) and (b) show the energy conditions  $\rho + P_r + 2P_t$  and  $\rho - P_r - 2P_t$ , respectively. These plots correspond to the solution of subject. 5.2 with  $\alpha = 0.2$ .

### 5.3 Solution II: mimic constraint for density

An alternative choice leading to a physically acceptable solution is the mimic constraint for the density (44); then, from eq. (10), we obtain

$$\rho = \bar{\rho}(1 + \alpha). \tag{66}$$

Then, equating eqs. (17) and (21) we get  $f^*(r)$ , which reads:

$$f^*(r) = \frac{B}{r} - \frac{3ar^2}{2} \frac{1 + c(1 + 4ar^2)^{-1/2}}{1 + ar^2}, \tag{67}$$

where the density  $\bar{\rho}$  from eq. (27) has been used. To avoid a singular behaviour at the center  $r = 0$  we must impose  $B = 0$ , then eq. (15) yields

$$e^{-\lambda(r)} = \mu(r) - \alpha \left( \frac{3ar^2}{2} \frac{1 + c(1 + 4ar^2)^{-1/2}}{1 + ar^2} \right). \tag{68}$$

Next, evaluating  $f^*(r)$  from eq. (67) at eqs. (22) and (23) we find the expressions for  $\Theta_1^1(r)$  and  $\Theta_2^2(r)$ :

$$\Theta_1^1 = \frac{3a}{2\kappa^2} \frac{(\sqrt{1 + 4ar^2} + c)(1 + 7ar^2)}{(1 + ar^2)^2 \sqrt{1 + 4ar^2}}, \tag{69}$$

$$\Theta_2^2 = \frac{3a}{2\kappa^2} \frac{\sqrt{1 + 4ar^2}(9ar^2 + 1) + 7ar^2c + c}{(1 + ar^2)^2 \sqrt{1 + 4ar^2}}. \tag{70}$$

With expressions (69) and (70) the radial and tangential pressures (11) and (12) are:

$$p_r(r) = \bar{p}(r) - \alpha \frac{3a}{2\kappa^2} \frac{(\sqrt{1 + 4ar^2} + c)(1 + 7ar^2)}{(1 + ar^2)^2 \sqrt{1 + 4ar^2}} \tag{71}$$

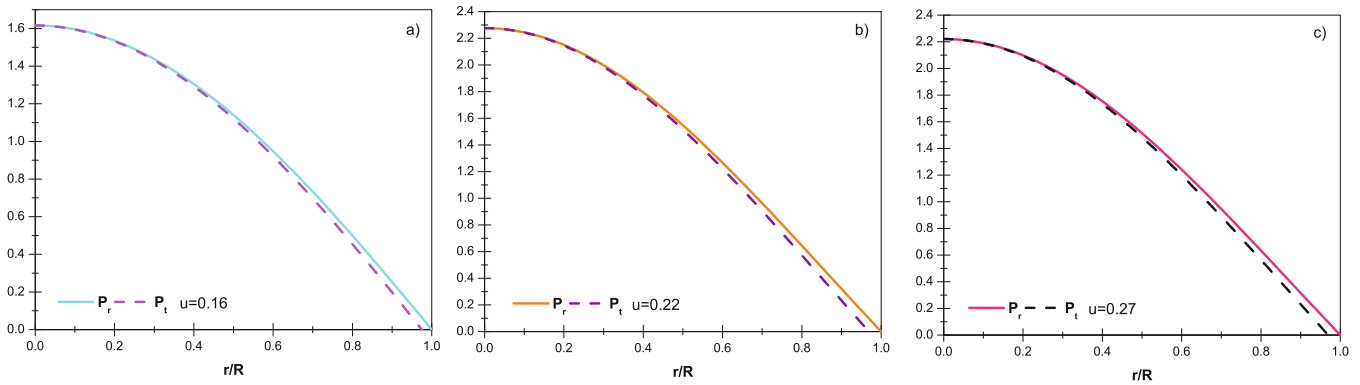


**Fig. 6.** The three panels display the tangential (lower curve) and the radial (upper curve) pressures, exhibiting a monotonically decreasing behaviour with the increasing  $r$ . All the above quantities are divided by the constant  $a$ , *i.e.*,  $P_r = p_r/a$  and  $P_t = p_t/a$ . These plots correspond to the solution of subject. 5.3 with  $\alpha = 0.3$ .

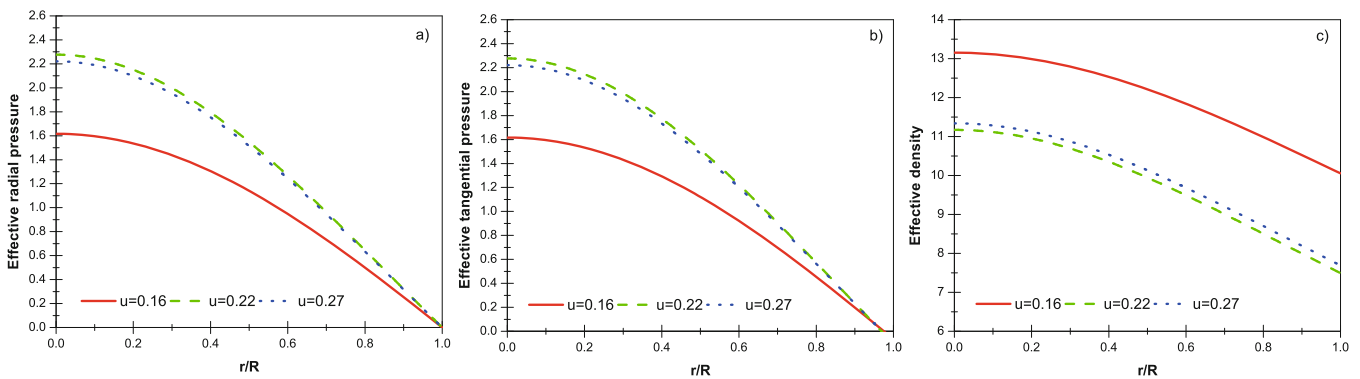


**Fig. 7.** Panel (a) shows the effective radial pressure. Panel (b) shows the effective tangential pressure and panel (c) shows the decreasing effective energy density. All these quantities are divided by the value of  $a$ . These plots correspond to the solution of subject. 5.3 with  $\alpha = 0.3$ .

and

$$p_t(r) = \bar{p}(r) - \alpha \frac{3a(\sqrt{1+4ar^2}(9ar^2+1) + (7ar^2+1)c)}{2\kappa^2(1+ar^2)^2\sqrt{1+4ar^2}}. \tag{72}$$

The continuity of the effective radial pressure (47), along with eq. (71), yields to

$$c = -\frac{\sqrt{1+4aR^2}(-3+3aR^2+\alpha+7\alpha aR^2)}{(1+\alpha)(1+7aR^2)}. \tag{73}$$

Using the expression given by (67), the matching conditions in (49) and (50) lead to

$$A^2(1+aR^2)^3 = 1 - \frac{2M}{R} \tag{74}$$

and

$$1 - (1+\alpha) \left( \frac{3ar^2}{2} \frac{1+c(1+4ar^2)^{-1/2}}{1+ar^2} \right) = 1 - \frac{2M}{R}. \tag{75}$$

Equations (73)–(75) are the necessary and sufficient conditions to match the exterior Schwarzschild solution with the deformed interior solution.

Inserting  $f^*(r)$  from eq. (67) and  $c$  from eq. (73) at eq. (75) we again find the same value for  $a$  from eq. (59). Next with this value for  $a$  we will obtain the value for  $c$  from eq. (73) and  $A$  from eq. (74).

For testing the admissibility of our solution we again choose the same values of mass and radius from subjects. 4 and 5.2 but now  $\alpha = 0.3$ , obtaining  $a$  from eq. (59) and  $c$  from eq. (73). For these values fig. 6 shows the radial pressure  $p_r(r)$  and tangential pressure  $p_t(r)$  inside the spherical distribution, showing how the magnitude of the anisotropy increases towards the surface. The tangential pressure is less than radial pressure, *i.e.*, there is an attractive force.

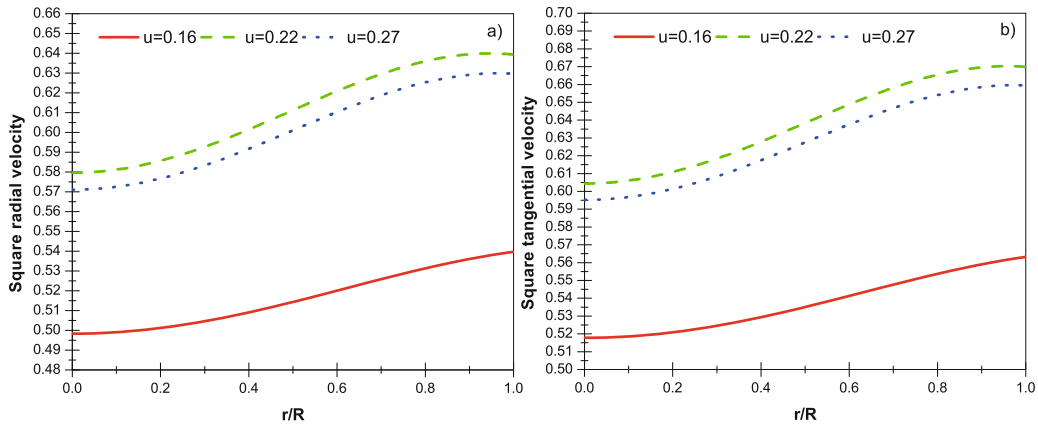


**Fig. 8.** Panels (a) and (b) show the squares of radial and tangential velocities respectively. These plots correspond to the solution of subject. 5.3 with  $\alpha = 0.3$ .

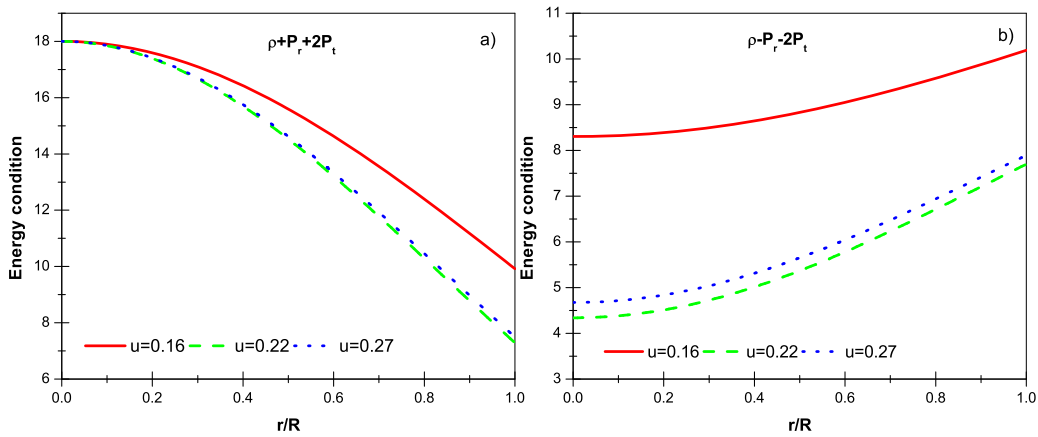


**Fig. 9.** Panels (a) and (b) show the energy conditions  $\rho + P_r + 2P_t$  and  $\rho - P_r - 2P_t$ , respectively. These plots correspond to the solution of subject. 5.3 with  $\alpha = 0.3$ .

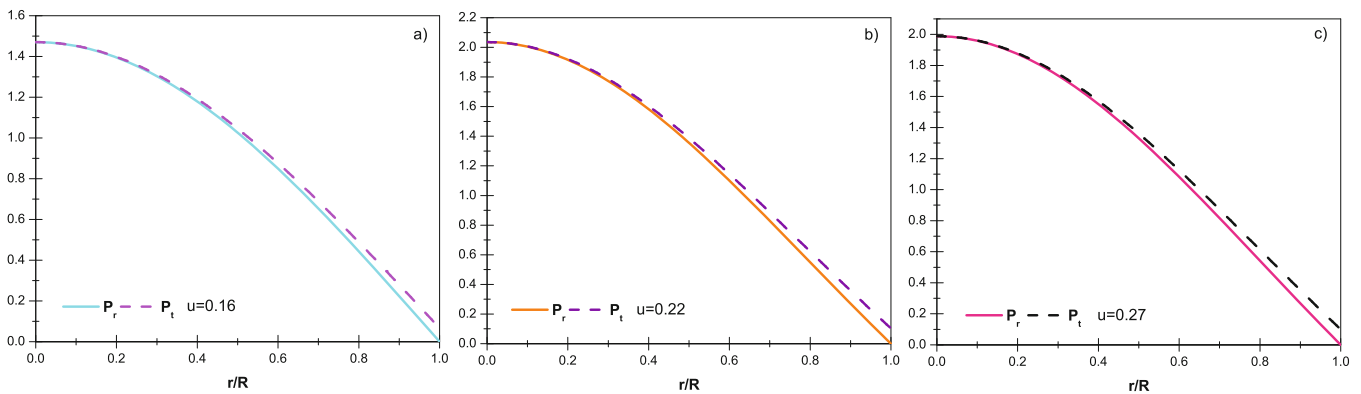


**Fig. 10.** The three panels display the radial (lower curve) and the tangential (upper curve) pressures, exhibiting a monotonically decreasing behaviour with the increasing  $r$ . All the above quantities are divided by the constant  $a$ , *i.e.*,  $P_r = p_r/a$  and  $P_t = p_t/a$ . These plots correspond to the solution of subject. 5.3 with  $\alpha = -0.3$ .

Also we observe that the tangential pressure becomes negative before the boundary. In figs. 6, 7, 8 and 9 we observe that all requirements of admissibility of subject. 5.1 are fulfilled.

With the same values of mass and radius it is also possible show a scenario where the tangential pressure is greater than radial pressure and being both positives, *i.e.*, there is a repulsive force, for example, with  $\alpha = -0.3$ . In figs. 10, 11, 12 and 13 we see, again, that all the admissibility conditions are fulfilled, therefore with  $\alpha = -0.3$  the solution is also well behaved.

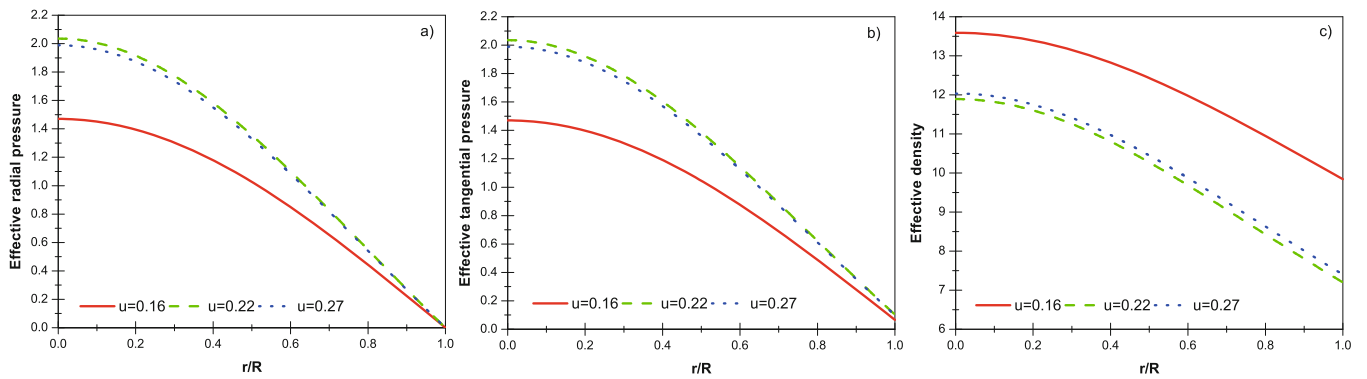


**Fig. 11.** Panel (a) shows the effective radial pressure. Panel (b) shows the effective tangential pressure and panel (c) shows the decreasing effective energy density. All these quantities are divided by the value of  $a$ . These plots correspond to the solution of subject. 5.3 with  $\alpha = -0.3$ .

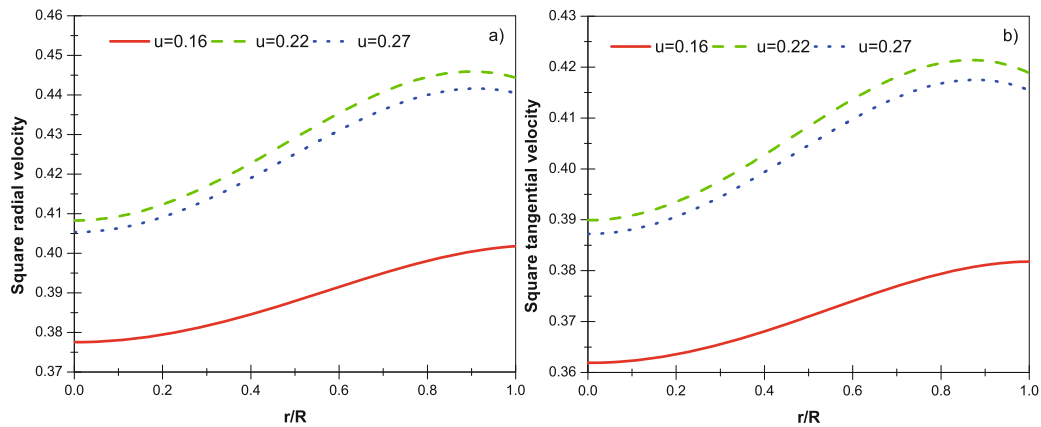


**Fig. 12.** Panels (a) and (b) show the squares of radial and tangential velocities, respectively. These plots correspond to the solution of subject. 5.3 with  $\alpha = -0.3$ .

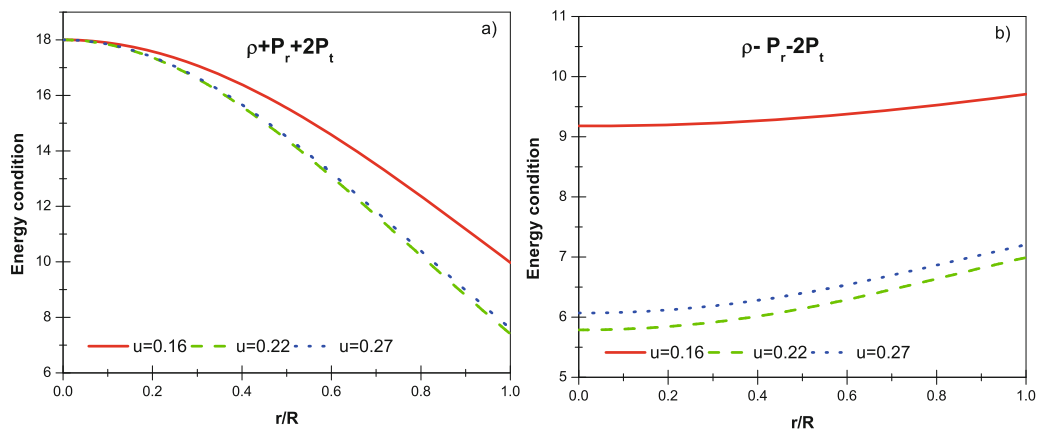


**Fig. 13.** Panels (a) and (b) show the energy conditions  $\rho + P_r + 2P_t$  and  $\rho - P_r - 2P_t$ , respectively. These plots correspond to the solution of subject. 5.3 with  $\alpha = -0.3$ .

### 5.4 Stability conditions

One important aspect in the study of compact objects in general relativity describing anisotropic matter distributions is the stability of the model. In this section we analyze the stability of the present model from two perspectives. The first one is via the adiabatic index  $\Gamma$  and the second one is through the analysis of the square of the sound speeds using Abreu *et al.* [32] studies based on Herrera’s cracking concept [33].

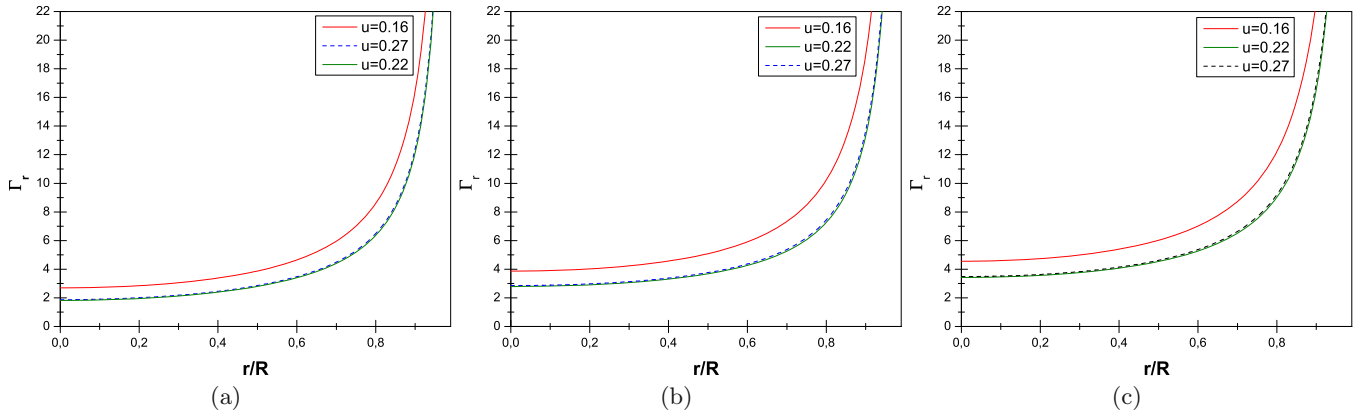


**Fig. 14.** Adiabatic index criterion: (a) Solutions of subject. 5.2. (b) Solutions of subject. 5.3 with  $\alpha = -0.3$ . (c) Solutions of subject. 5.3 with  $\alpha = 0.3$ .

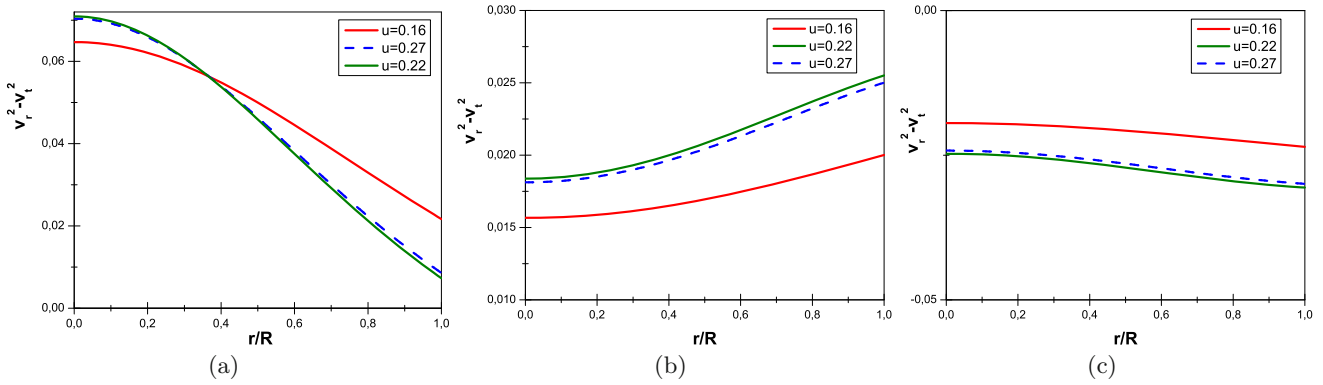


**Fig. 15.** Abreu criterion  $v_r^2 - v_t^2$ : (a) Solutions of subject. 5.2. (b) Solutions of subject. 5.3 with  $\alpha = -0.3$ . (c) Solutions of subject. 5.3 with  $\alpha = 0.3$ .

It is well known that a spherically symmetric and static configuration associated with a Newtonian isotropic matter distribution will collapse if the adiabatic index is  $\Gamma < 4/3$ . In distinction with the relativistic anisotropic fluid spheres the collapsing condition becomes [34, 35]

$$\Gamma < \frac{4}{3} + \left[ \frac{1}{3} \kappa \frac{\rho_0 p_{r0}}{|p'_{r0}|} r + \frac{4}{3} \frac{(p_{t0} - p_{r0})}{|p'_{r0}| r} \right]_{\max}, \tag{76}$$

where  $\rho_0$ ,  $p_{r0}$  and  $p_{t0}$  are the initial density, radial and tangential pressure when the fluid is in static equilibrium. The second term in the right-hand side represents the relativistic corrections to the Newtonian perfect fluid and the third term is the contribution due to anisotropy. Heintzmann and Hillebrandt [36] showed that the stability condition for a relativistic compact object is given by  $\Gamma > 4/3$ . Since the gravitational collapse takes place in the radial direction of the configuration it is sufficient to calculate the adiabatic index  $\Gamma_r$  in such direction. We can explicitly obtain the adiabatic index from, [37]

$$\Gamma_r = \frac{\rho + p_r}{p_r} \frac{dp_r}{d\rho}. \tag{77}$$

Figure 14 shows that all our models satisfy the above criteria. Therefore it is a stable model. On the other hand, Abreu *et al.* analysis regarding the square of the sound speeds within the stellar configuration, provides us a criteria to determine the regions where the model is stable. So the model is stable if  $v_r^2 - v_t^2$  remains between 0 and 1 and unstable if  $v_r^2 - v_t^2$  remains between  $-1$  and  $0$ . We can see that the solutions of figs. 15(a) and (b) become potentially stable since they fulfill the condition  $0 < v_r^2 - v_t^2 < 1$ , whereas the solutions of fig. 15(c) become unstable.

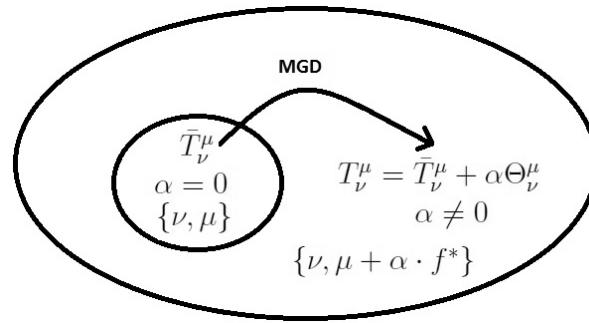


**Fig. 16.** Minimal geometric deformation approach.

**Table 1.** Energy density and central pressure in the CGS system.

Solution	$u$	$\alpha$	$a$ ( $\text{cm}^{-2}$ )	$c$ (dimensionless)	Central density ( $\text{g}/\text{cm}^3$ )	Surface density ( $\text{g}/\text{cm}^3$ )	Central pressure ( $\text{dyne}/\text{cm}^2$ )
Section 4	0.163	0	$1.422 \cdot 10^{-13}$	1.969	$1.018 \cdot 10^{15}$	$7.57 \cdot 10^{14}$	$1.06 \cdot 10^{35}$
	0.222	0	$4.287 \cdot 10^{-13}$	1.551	$2.634 \cdot 10^{15}$	$1.672 \cdot 10^{15}$	$4.49 \cdot 10^{35}$
	0.27	0	$2.756 \cdot 10^{-13}$	1.151	$1.43 \cdot 10^{15}$	$7.612 \cdot 10^{14}$	$3.683 \cdot 10^{35}$
Subsection 5.2	0.163	0.2	$1.422 \cdot 10^{-13}$	1.969	$1.089 \cdot 10^{15}$	$7.324 \cdot 10^{14}$	$8.48 \cdot 10^{34}$
	0.222	0.2	$4.287 \cdot 10^{-13}$	1.551	$2.934 \cdot 10^{15}$	$1.598 \cdot 10^{15}$	$3.592 \cdot 10^{35}$
	0.27	0.2	$2.756 \cdot 10^{-13}$	1.151	$1.676 \cdot 10^{15}$	$7.195 \cdot 10^{14}$	$2.946 \cdot 10^{35}$
Subsection 5.3	0.163	0.3	$1.422 \cdot 10^{-13}$	1.246	$1.001 \cdot 10^{15}$	$7.653 \cdot 10^{14}$	$5.551 \cdot 10^{34}$
	0.222	0.3	$4.287 \cdot 10^{-13}$	0.9	$2.552 \cdot 10^{15}$	$1.706 \cdot 10^{15}$	$2.371 \cdot 10^{35}$
	0.27	0.3	$2.756 \cdot 10^{-13}$	0.558	$1.348 \cdot 10^{15}$	$7.878 \cdot 10^{14}$	$1.966 \cdot 10^{35}$
	0.163	-0.3	$1.422 \cdot 10^{-13}$	3.311	$1.035 \cdot 10^{15}$	$7.489 \cdot 10^{14}$	$5.049 \cdot 10^{34}$
	0.222	-0.3	$4.287 \cdot 10^{-13}$	2.761	$2.722 \cdot 10^{15}$	$1.638 \cdot 10^{15}$	$2.119 \cdot 10^{35}$
	0.27	-0.3	$2.756 \cdot 10^{-13}$	2.251	$1.513 \cdot 10^{15}$	$7.345 \cdot 10^{14}$	$1.717 \cdot 10^{35}$

## 6 Conclusions and remarks

We showed that by imposing our matching conditions the isotropic Heintzmann's solution is well behaved using typical mass and radius values for some compact objects such as 4U 1538-52, RXJ 1856-37 and Vela X-1, whose compactness factors  $u$  are 0.16, 0.22 and 0.27, respectively. The choice of the Heintzmann IIa solution is merely arbitrary, because there is no evidence that the mentioned compact stars are described fully by this solution.

Then, applying the Minimal Geometric Deformation method to Heintzmann's solution we have found two new analytic anisotropic and spherically symmetric solutions of Einstein field equations. These two solutions are the results of the decoupling of Einstein equations in a isotropic sector described by  $\bar{T}_{\mu\nu}$  and the sector described by the quasi-Einstein equations with a source  $\Theta_{\mu\nu}$ . Due to the application of MGD the perfect and the extra fluid are separately conserved. So, the combination of these two sectors has only gravitational interaction, and does not has exchange of energy momentum.

We have shown that these two new solutions are well behaved for the above parameters of mass and radius, since they fulfill every admissibility criteria of the subsect. 5.1. To accomplish it we use  $\alpha = 0.2$  and  $\alpha = 0.3$  in the first and second constraint, respectively. Moreover, considering  $\alpha = 0.3$  in the second constraint, we obtained an attractive force where the tangential pressure becomes negative before the boundary of the compact object, but using  $\alpha = -0.3$  a repulsive force appears. In all cases the solutions are well behaved. The matching conditions are perfectly satisfied in both solutions.

All the sources  $\Theta_{\mu\nu}$  used in this work are generic gravitational sources, therefore they do not represent a high density equation of state *i.e.* they do not impose that the tangential pressure is positive inside the fluid sphere.

In fig. 16 we observe how any perfect fluid solution can be consistently extended to the anisotropic domain via the MGD approach. In our case the seed well behaved Heintzmann's solution  $\{\nu, \mu\}$  is extended to an anisotropic well behaved scenario  $\{\nu, \mu + \alpha \cdot f^*\}$ .

In this work we do not make a complete study about compact objects, however our solutions would serve for future studies about these objects. Moreover, working in the CGS system table 1 shows the values of the central and surface energy density and central pressure, corresponding to the isotropic Heintzmann's solution from sect. 4 and both anisotropic extensions from subsect. 5.2 (mimic constraint for pressure) and from subsect. 5.3 (mimic constraint for density). We found values for central and surface density of the order of  $10^{14}$ – $10^{15}$   $\text{g}/\text{cm}^3$  and central pressure of the order of  $10^{34}$ – $10^{35}$   $\text{dyne}/\text{cm}^2$ . These are typical values for compact objects, some examples can be found in refs. [8, 9, 38].

ME was partially funded by FONDECYT Regular under Grant No. 1151107. FT-O thanks the financial support of the ANT-1755 project at the Universidad de Antofagasta-Chile.

## References

1. M.K. Mak, T. Harko, *Chin. J. Astron. Astrophys.* **2**, 248 (2002).
2. M.K. Mak, T. Harko, *Proc. R. Soc. London A* **459**, 393 (2003).
3. K.N. Singh, N. Pant, M. Govender, *Indian J. Phys.* **90**, 1215 (2016).
4. S.K. Maurya, Y.K. Gupta, Saibal Ray, Debabrata Deb, *Eur. Phys. J. C* **76**, 693 (2016).
5. S.K. Maurya, *Eur. Phys. J. A* **53**, 89 (2017).
6. B.V. Ivanov, *Eur. Phys. J. C* **77**, 738 (2017).
7. M.K. Jasim, S.K. Maurya, Y.K. Gupta, *Astrophys. Space Sci.* **361**, 352 (2016).
8. S.K. Maurya, Y.K. Gupta, Baiju Dayanandan, Saibal Ray, *Eur. Phys. J. C* **76**, 266 (2016).
9. Piyali Bhar, Ksh. Newton Singh, Tuhina Manna, *Int. J. Mod. Phys. D* **26**, 1750090 (2017).
10. S. Thirukkanesh, F.C. Ragel, Ranjan Sharma, Shyam Das, *Eur. Phys. J. C* **78**, 31 (2018).
11. L. Herrera, J. Ospino, A. Di Prisco, *Phys. Rev. D* **77**, 027502 (2008).
12. M. Chaisi, S.D. Maharaj, *Pramana* **66**, 313 (2006).
13. J. Ovalle, *Phys. Rev. D* **95**, 104019 (2017).
14. J. Ovalle, *Mod. Phys. Lett. A* **23**, 3247 (2008).
15. J. Ovalle, *Braneworld Stars: Anisotropy Minimally Projected Onto the Brane*, in *Proceedings of the Ninth Asia-Pacific International Conference* (Singapore, 2009) p. 173–182.
16. Roberto Casadio, J. Ovalle, Roldao da Rocha, *Class. Quantum Grav.* **32**, 215020 (2015).
17. J. Ovalle, *Int. J. Mod. Phys. Conf. Ser.* **41**, 1660132 (2016).
18. J. Ovalle, F. Linares, *Phys. Rev. D* **88**, 104026 (2013).
19. J. Ovalle, Laszl A. Gergely, Roberto Casadio, *Class. Quantum Grav.* **32**, 045015 (2015).
20. Roberto Casadio, J. Ovalle, Roldao da Rocha, *EPL* **110**, 40003 (2015).
21. L. Gabbanelli, A. Rincon, C. Rubio, *Eur. Phys. J. C* **78**, 370 (2018).
22. J. Ovalle, R. Casadio, R. da Rocha, A. Sotomayor, *Eur. Phys. J. C* **78**, 122 (2018).
23. Delgaty, Kayll Lake, *Comput. Phys. Commun.* **115**, 395 (1998).
24. H. Heintzmann, *Z. Phys.* **228**, 489 (1969).
25. N. Pant, R.N. Mehta, M. Pant, *Astrophys. Space Sci.* **332**, 473 (2011).
26. K.N. Singh, N. Pant, *Indian J. Phys.* **90**, 843 (2016).
27. Cristiano Germani, Roy Maartens, *Phys. Rev. D* **64**, 124010 (2001).
28. Herrera, N.O. Santos, *Phys. Rep.* **286**, 53 (1997).
29. George Ellis, Roy Maartens, Malcolm MacCallum, *Gen. Relativ. Gravit.* **39**, 1651 (2007).
30. Private communication with Luis Herrera
31. Private communication with Tiberiu Harko.
32. H. Abreu, H. Hernandez, L.A. Nunez, *Class. Quantum Grav.* **24**, 4631 (2007).
33. L. Herrera, *Phys. Lett. A* **165**, 206 (1992).
34. R. Chan, L. Herrera, N.O. Santos, *Mon. Not. R. Astron. Soc.* **265**, 533 (1993).
35. R. Chan, L. Herrera, N.O. Santos, *Mon. Not. R. Astron. Soc.* **267**, 637 (1994).
36. H. Heintzmann, W. Hillebrandt, *Astron. Astrophys.* **38**, 51 (1975).
37. R. Chan, S. Kichenassamy, G. Le Denmat, N.O. Santos, *Mon. Not. R. Astron. Soc.* **239**, 91 (1989).
38. S.K. Maurya, Y.K. Gupta, Saibal Ray, Baiju Dayanandan, *Eur. Phys. J. C* **75**, 225 (2015).